

600 W power scalable single transverse mode tapered double-clad fiber laser

V. Filippov,^{1*} Y. Chamorovskii,² J. Kerttula¹, A. Kholodkov² and O. G. Okhotnikov¹

¹Optoelectronics Research Centre, Tampere University of Technology, 33101 Tampere, Finland

²Institute of Radio and Electronics of the Russian Academy of Sciences, Mokhovaya 11, bld.7, 125009 Moscow, Russia

*Corresponding author: valery.filippov@tut.fi

Abstract: Pump propagation and absorption in active tapered double-clad fiber has been analyzed based on a ray optics approach. Optimization of the longitudinal shape, absorption and angular distribution of the pump beam allowed for power scaling of a ytterbium fiber laser up to 600 W with high beam quality ($M^2 \leq 1.08$) and a slope efficiency of 63%. It is shown that the influence of vignetting in a tapered fiber can be avoided, resulting in high overall efficiency, in good agreement with the presented model.

©2009 Optical Society of America

OCIS codes: (060.2280) Fiber design and fabrication; (060.2320) Fiber optics amplifiers and oscillators; (060.3510) Lasers, fiber

References and links

1. www.ipgphotonics.com
2. S. Gray, A. Liu, D. T. Walton, J. Wang, M. Li, X. Chen, A. B. Ruffin, J. A. DeMeritt, and L. A. Zenteno, "502 Watt, single transverse mode, narrow linewidth, bidirectionally pumped Yb-doped fiber amplifier," *Opt. Express* **15**, 17044-17050 (2007), <http://www.opticsinfobase.org/oe/abstract.cfm?URI=oe-15-25-17044>.
3. Y. Jeong, J. Sahu, D. Payne, and J. Nilsson, "Ytterbium-doped large-core fiber laser with 1.36 kW continuous-wave output power," *Opt. Express* **12**, 6088-6092 (2004), <http://www.opticsinfobase.org/oe/abstract.cfm?URI=oe-12-25-6088>.
4. G. Bonati, H. Voelckel, T. Gabler, U. Krause, A. Tunnermann, J. Limpert, A. Liem, T. Schreiber, S. Nolte and H. Zellmer, "1.53 kW from a single mode Yb-doped crystal fiber laser," *Photonics West, Late Breaking Developments, Session 5709-2a (The International Society for Optical Engineering, 2005)*.
5. V. Filippov, Y. Chamorovskii, J. Kerttula, K. Golant, M. Pessa, and O. G. Okhotnikov, "Double clad tapered fiber for high power applications," *Opt. Express* **16**, 1929-1944 (2008), <http://www.opticsinfobase.org/abstract.cfm?URI=oe-16-3-1929>.
6. V. Filippov, Y. Chamorovskii, J. Kerttula, A. Kholodkov, and O. G. Okhotnikov, "Single-mode 212 W tapered fiber laser pumped by a low-brightness source," *Opt. Lett.* **33**, 1416-1418 (2008), <http://www.opticsinfobase.org/ol/abstract.cfm?URI=ol-33-13-1416>.
7. V. Filippov, Y. Chamorovskii, J. Kerttula, A. Kholodkov, and O. G. Okhotnikov, "High power tapered ytterbium fiber laser pumped by a low-brightness source," 3rd EPS-QEOD Europhoton Conference on Solid-State, Fiber and Waveguided Light Sources, 31 August – 05 September 2008, Paris (France), Europhysics Conference Abstract vol.32G, ISBN: 2-914771-55-X, paper TUoC.3, p. 33.
8. N. S. Kapany and J. J. Burke, *Optical waveguides* (Academic Press, New York, 1972).
9. V. B. Veinberg and D. K. Sattarov, *Waveguide Optics* (Mashinostroenie, Leningrad, 1977), Chap.5 (in Russian).
10. <http://www.laserline.de/>
11. J. Limpert, N. Deguil-Robin, I. Manek-Hönninger, F. Salin, F. Röser, A. Liem, T. Schreiber, S. Nolte, H. Zellmer, A. Tünnermann, J. Broeng, A. Petersson, and C. Jakobsen, "High-power rod-type photonic crystal fiber laser," *Opt. Express* **13**, 1055-1058 (2005), <http://www.opticsinfobase.org/oe/abstract.cfm?URI=oe-13-4-1055>.
12. L. Michaille, C. R. Bennett, D. M. Taylor, T. J. Shepherd, J. Broeng, H. R. Simonsen, and A. Petersson, "Phase locking and supermode selection in multicore photonic crystal fiber lasers with a large doped area," *Opt. Lett.* **30**, 1668-1670 (2005), <http://www.opticsinfobase.org/ol/abstract.cfm?URI=ol-30-13-1668>.

1. Introduction

The technology of high power fiber lasers and amplifiers has undergone a significant progress during last decade. These devices are either side-pumped by large number of relatively low

power (~ 10 W) fiber coupled diodes through pump combiners or end-pumped by diode bars through the end face of an active double clad fiber [1-2]. The highest output power demonstrated to date (1.36 kW in [3] and 1.53 kW in [4]) has been achieved with diode bars producing kilowatt level pump power and low brightness beam. The end pumped configuration usually implements the large mode area (LMA) active double clad fiber with clad diameter of 400-600 μm . The pump absorption in the double clad fibers proportional to the core/clad area ratio which is typically in a range of $2.5 \times (10^{-3} \div 10^{-2})$. It should be noted that this approach has an intrinsic limitation determined by the trade-off between core and clad size. Indeed, since the core diameter is determined by the fundamental mode operation, the clad diameter cannot be increased considerably without reducing the pump absorption. Therefore, the clad diameter imposes eventually the limitation on the launched pump power and, consequently, on the output power of the end-pumped fiber laser.

Recently, we have proposed an active tapered double-clad fiber (T-DCF) as a gain medium for high power fiber lasers and amplifiers [4-7]. T-DCF was shown to have several distinct advantages as compared with regular fibers, particularly, it can be pumped with low brightness sources and offers an efficient intrinsic mode mixing mechanism resulting in enhanced pump absorption and robust single mode generation.

It should be mentioned that longitudinally irregular T-DCF generally exhibits additional loss of pump radiation owing to leakage to the cladding. Indeed, pump propagation in the cladding of tapered double-clad fiber is accompanied by a gradual increase of propagation angle relative to the fiber axis. As a result, when the condition of total internal reflection is violated, some rays leak to the pump cladding, leading to the so-called vignetting effect [8, 9]. The total pump power balance, therefore, includes pump absorbed by the active core, pump which passes through the fiber unabsorbed and appears at the small-core end of the taper as residual pump, and pump radiation which leaks out of the fiber. The pump power absorption can therefore not be estimated from the launched and unabsorbed pump power ratio, which is the usual method applied in the case of regular fibers. A model of pump propagation/absorption in tapered active fiber allowing accurate optimization of T-DCF operation has not been available until now.

In this paper, we present a theoretical model of tapered active fiber which provides an adequate tool for T-DCF optimization. Over 600 W output power in the fundamental spatial mode regime has been demonstrated. Good agreement with theoretical predictions suggests that a further increase of output power would be possible.

2. Theoretical model

The conceptual structure of T-DCF is shown in Fig. 1 (a). It contains a core doped with rare earth ions, a cladding with index of refraction n_{clad} , where the pump emission propagates, and an outer cladding with low index of refraction. The diameter of T-DCF gradually decreases toward the narrow end, which ensuring single mode propagation regime.

The pump propagation throughout an active T-DCF has been analyzed using ray optics, taking into account meridional rays. The essential difference of T-DCF, as compared with regular fiber, is a gradual increase of the propagation angle relative to the fiber axis, shown in Fig. 1 (a). Eventually, the propagation angle exceeds the critical angle for total internal reflection, resulting in pump leakage (refraction) into the secondary cladding, which is known as the vignetting phenomenon [7, 8]. We consider the propagation of meridional rays through a taper whose diameter has a linear dependence on the axial length L , with the diameters of the wide and narrow ends being D_1 and D_2 , respectively (Fig. 1 (a)).

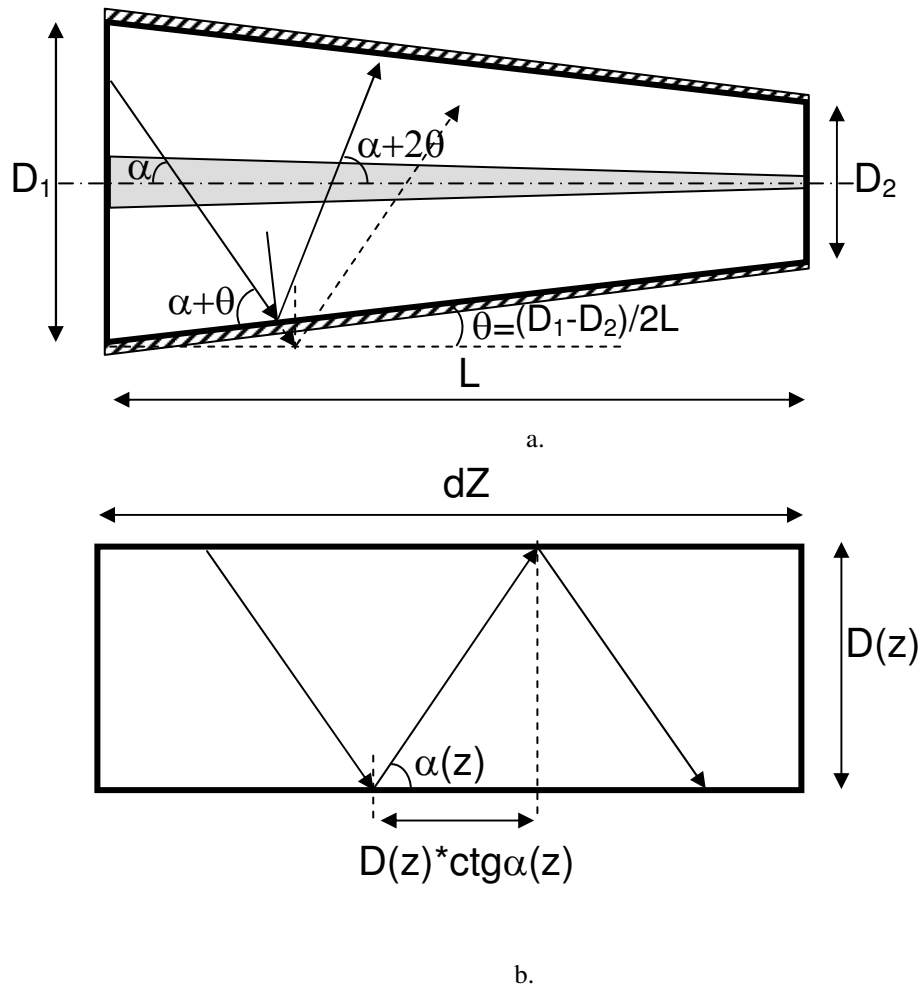


Fig. 1. Ray trajectory in: (a) tapered fiber and (b) cylindrical fiber.

The angle of linear taper is given by

$$\theta = \frac{D_1 - D_2}{2L} \quad (1)$$

and the diameter of the taper as a function of length can be written as

$$D(z) = D_1 - 2\theta \cdot z, \quad (2)$$

where z – is the axial coordinate of the tapered fiber.

Meridional rays propagating in a regular cylindrical fiber without undergoing refraction are reflected repeatedly at the boundary between two media of different refractive indices; the angles of reflection are always equal to the angles of incidence when they exceed the critical angle (Fig. 1 (b)). To the contrary, the angle of reflection in a linear taper increases after each reflection, by a value of 2θ . The ray changes its angle with the propagation length according to

$$\alpha(z) = \frac{\alpha_{in}}{n_{clad}} + 2\theta \cdot \eta(z), \quad (3)$$

where α_{in} – is the angle of incidence onto the taper, n_{clad} is the cladding refractive index and $\eta(z)$ is the number of multiple reflections in the taper occurring before the propagation distance z .

The angle θ is small, typically a few microradians, therefore, a tapered fiber with infinitesimal length dZ can be approximated by a cylindrical shape [8, 9]. The total number of reflections $\eta(z)$ of a ray propagating with the angle $\alpha(z)$ within a taper of length dZ and diameter $D(z)$ (see Fig.1 (b)) can then be approximated by

$$d\eta = \frac{dz}{D(z)} \operatorname{tg} \alpha(z). \quad (4)$$

Combining equations (2), (3) and (4) we can obtain an equation for the number of meridional ray reflections in a circular linear taper

$$\frac{d\eta}{\operatorname{tg}\left(\frac{\alpha_{in}}{n_{clad}} + 2\theta \cdot \eta\right)} = \frac{dz}{D_1 - 2\theta \cdot z}. \quad (5)$$

To calculate the total number of reflections in a linear taper, one should integrate Eq.(5)

$$\eta(z) = \frac{a \sin\left(\frac{D_1 \cdot \sin\left(\frac{\alpha_{in}}{n_{clad}}\right)}{D_1 - 2\theta \cdot z}\right) - \frac{\alpha_{in}}{n_{clad}}}{2\theta}. \quad (6)$$

Substituting Eq. (6) into (3) yields an expression for the meridional ray angle after a propagation distance z in a linear taper

$$\alpha(z) = a \sin\left(\frac{D_1 \cdot \sin\left(\frac{\alpha_{in}}{n_{clad}}\right)}{D_1 - 2\theta \cdot z}\right). \quad (7)$$

Equation (7) can be simplified for a total taper length L to yield

$$\alpha = a \sin\left(\frac{D_1}{D_2} \sin\left(\frac{\alpha_{in}}{n_{clad}}\right)\right) = a \sin\left(T \sin\left(\frac{\alpha_{in}}{n_{clad}}\right)\right), \quad (8)$$

where $T = D_1/D_2$ is the tapering ratio.

The ray propagates throughout the taper without vignetting when the condition $n_{clad} \times \sin \alpha < NA_{clad}$ is satisfied over the whole length of the taper. The product $n_{clad} \times \sin \alpha$ gradually increases with light propagation towards the small diameter single mode end of the taper and approaches the value of the cladding numerical aperture NA_{clad} only at the very end of the taper. The critical incident angle, which ensures ray propagation without vignetting, can then be found from

$$\sin\left(\frac{\alpha_{in}}{n_{clad}}\right) = \frac{1}{T} \cdot \frac{NA}{n_{clad}}, \quad (9a)$$

or, for paraxial rays (small values of α_{in}), from

$$\alpha_{in} \approx \frac{NA}{T} \quad (9b)$$

Equations (9a), (b) are valid for a tapered fiber with an arbitrary longitudinal dependence of taper diameter. Indeed, a T-DCF with nonlinear complex shape can be represented by a sequence of small-length linear tapers. Using Eq. (8), the ray angle after propagation through the chain of linear tapers with arbitrary shape can be approximated by

$$\alpha = \frac{\alpha_{in}}{n_{clad}} \cdot \frac{d_1}{d_2} \cdot \frac{d_2}{d_3} \cdot \dots \cdot \frac{d_{n-2}}{d_{n-1}} \cdot \frac{d_{n-1}}{d_n} = T \cdot \frac{\alpha_{in}}{n_{clad}}, \quad (10)$$

where d_i is the diameter of an elementary short linear taper.

When the condition $n_{clad} \sin \alpha < NA_{clad}$ is violated over a certain length of the taper, the normalized length $\left(\frac{z}{L}\right)_{vgnt}$ of linear taper where this inequality is not satisfied and where, therefore, the vignetting occurs, can be expressed as a function of ray incidence angle α_{in} using Eq.(7)

$$\left(\frac{z}{L}\right)_{vgnt} = \frac{T}{T-1} \left(1 - \frac{n_{core} \sin\left(\frac{\alpha_{in}}{n_{core}}\right)}{NA} \right). \quad (11)$$

The similar dependence for an arbitrarily shaped taper can be found for an actual T-DCF axial profile by approximating it by a sequence of linear tapers and using Eq. (7) for each fractional taper. The dependence of diameter on length and an end face image for the T-DCF used in the experiments are shown in Figs. 2 (a) and 2 (b), respectively.

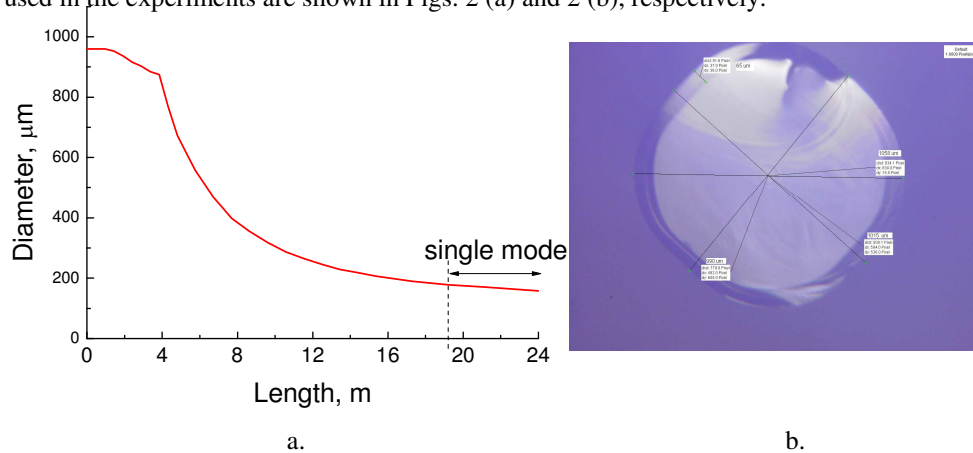


Fig. 2. T-DCF characteristics: (a) clad diameter versus length and (b) image of taper end face.

The numerical aperture of the pump cladding is 0.22 and the tapering ratio $T=6$, as defined in (8). According to (9), rays launched into the taper with incident angles below 0.037 rad ($NA/T \sim 0.22/6$) are expected to propagate without vignetting over the entire length of the taper. Rays launched at angles above 0.037 rad will be partially absorbed by the active core, and in part leak from the T-DCF cladding, due to vignetting. To quantify the amount of pump absorption and loss due to leakage from a taper, the characterization of the T-DCF has been performed for pump launch conditions which prevent vignetting. The practical beam delivery system used in this measurement employs launch optics to deliberately underfill the fiber aperture, by limiting the numerical aperture of the input pump beam to $NA \leq 0.037$. The pump absorption measured for rays with an aperture less than NA/T can be regarded as *paraxial ray pump absorption*.

The measured paraxial ray absorption for the T-DCF presented in Fig. 2(a), (b) which was used in this study was 1.2 dB/m at 915 nm, with an actual numerical aperture of pump light launched into the pump cladding of 0.0377.

The normalized length of vignetting for a T-DCF with arbitrary shape as function of launching angle can be calculated using the model of short-length linear tapers sequence, and applying it to each taper Eq. (8). The result of these calculations for the fabricated T-DCF is shown in Fig. 3.

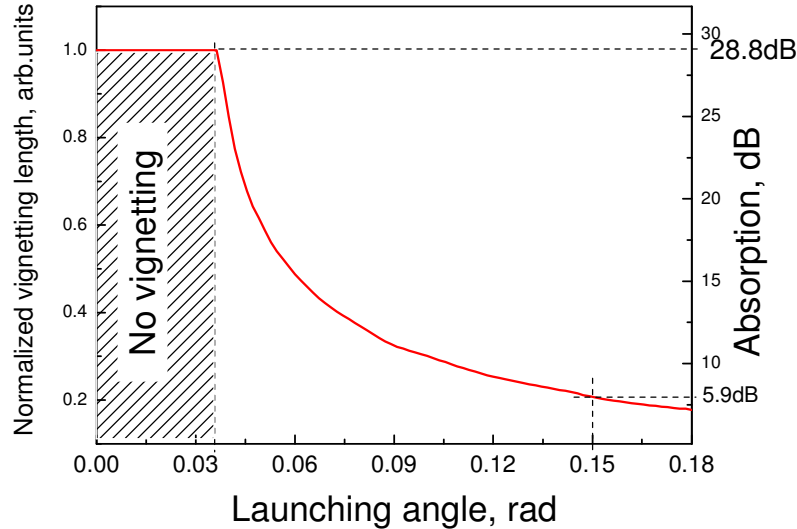


Fig. 3. Normalized vignetting length (left) and absorption (right) in T-DCF as a function of the launching angle.

Figure 3 illustrates that vignetting depends strongly on the incident angle of the cone of rays launched into the T-DCF. Since vignetting decreases pump absorption in the taper core, which is proportional to the propagation length, the pump efficiency reduces with increasing numerical aperture of the pump beam. Strong angular selectivity of the double clad taper absorption results in ~ 23 dB increase in absorption for beams with $NA < 0.037$ rad, compared with absorption for beams with $NA = 0.15$, corresponding to the overfill launching condition. The above analysis has been developed for taper excitation by a ray with a specific launching angle. In practice, however, the pump source produces a cone of rays with a Lorentzian angular power distribution. The measured angular power distributions for the launching optics, providing pump beam numerical apertures of 0.15 and 0.18, are shown in Figs. 4 (a) and 4 (b), respectively (black curves). The corresponding normalized angular distributions of absorbed pump power shown in Fig. 4 (a), (b) (red curves) have been calculated by taking into

account the dependence of pump absorption on the launching angle, presented in Fig. 3, and the angular pump power distribution shown, in Fig. 4.

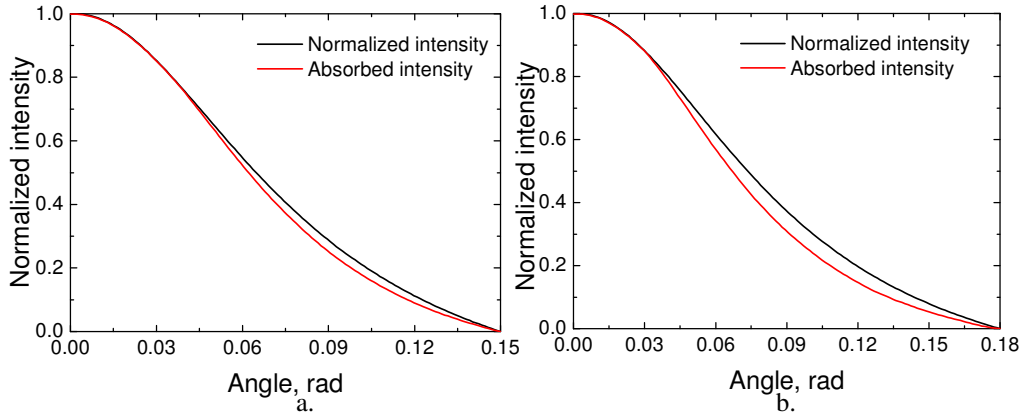


Fig. 4. Measured angular power distribution of pump sources with NA=0.15 (a) and NA=0.18 (b) and pump absorption (red curves).

Absorbed pump power, and pump power which is lost due to vignetting as a function of pump NA, can be calculated from the equations

$$P_{abs} = \frac{\int (P(\alpha) - P(\alpha) \exp(-\gamma L(\alpha))) d\alpha}{\int P(\alpha) d\alpha}, \quad (12a)$$

$$P_{vgnt} = 1 - P_{abs} - P_{unabs} \quad (12b)$$

where $P(\alpha)$ – angular power distribution of pump source, $L(\alpha)$ – vignetting length for ray, launched at the angle α , γ – absorption of double-clad taper per unit length for $\alpha \leq NA/T$, P_{unabs} – residual unabsorbed pump power transmitted throughout the T-DCF to the narrow end.

The pump absorption as a function of pump beam NA has been calculated using Eq.12(a) for the T-DCF with a diameter variation with length presented in Fig. 2. Fig. 5 demonstrates 15 dB (97%) absorption for a pump source with NA=0.15 and 1.2 dB/m paraxial ray absorption, which illustrates the tapered double-clad fiber's ability to pump absorption.

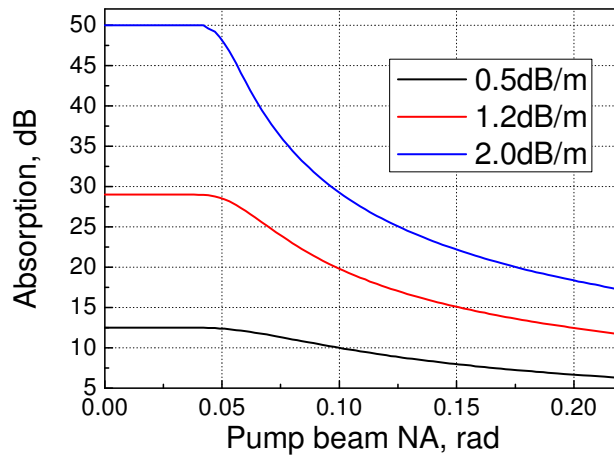


Fig. 5. Pump absorption in T-DCF versus numerical aperture of launched pump beam for actual shape of T-DCF and paraxial ray absorption of 0.2 dB/m (black), 1.2 dB/m (red) and 2 dB/m (blue).

A brief summary of the model presented above allows parameters determining the performance of tapered double-clad fiber lasers/amplifiers to be identified:

- Paraxial ray absorption;
- Shape of the taper;
- Angular power distribution of the pump source.

Importantly, the detrimental effect of vignetting can be largely suppressed by optimizing the shape of the taper, increasing paraxial ray absorption and using a pump beam with proper numerical aperture.

3. Experiment

The laser setup of the single mode ytterbium fiber laser with T-DCF as a gain medium is shown in Fig. 6. The diode source LDM 600-1500 (Laserline) operated at 915 nm provides pump radiation through an optical fiber with 600 μm core diameter and $\text{NA}=0.22$.

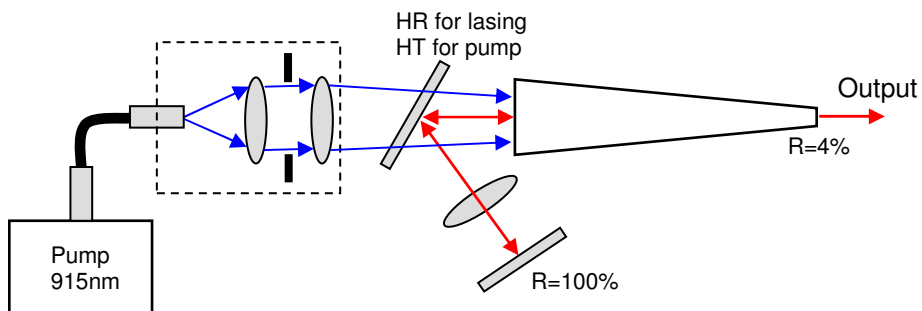


Fig. 6. The experimental setup

The maximum achievable power from this source was 1.3 kW. The output pump radiation was launched via optical cable into a beam shaping unit comprising a collimating lens,

diaphragm and focusing lens. The launched beam with Lorentzian intensity profile, as shown in Fig. 4 (a), (b), could be produced using simple coupling optics. By changing the lenses and the diaphragm we could adjust the numerical aperture and diameter of the pump beam launched into the T-DCF. The pump radiation was launched into the T-DCF through a dichroic beam splitter highly transparent for pump radiation and highly reflective for the lasing wavelength. The pump emission launch efficiency was 86%. The cavity was formed by a highly reflective dielectric mirror at the wide end of the T-DCF and by Fresnel reflections (~4%) from the facet of the narrow end. The total T-DCF length was 24 m, as shown in Fig. 2 (a). The fiber had a near-circular cladding cross-section, with the diameter at the wide side of the T-DCF varying in the range 835 - 890 μm , as shown in Fig. 2 (b). The fluorine glass coating with a NA of 0.22 was deposited on the pump guiding cladding. A low refractive index polymer was used for outer protection. The active core with a numerical aperture of 0.07 had a diameter of 65 μm at the wide end of the T-DCF. The core diameter at the narrow end of the taper was 11 μm , ensuring that at least five meters of the T-DCF was a single mode waveguide. The preform for the tapered fiber was fabricated by a plasma chemical vapor deposition (PCVD) method with in-core absorption of ~600 dB/m at 976 nm. As mentioned earlier, the paraxial ray absorption of double-clad pumped taper was measured to be 1.2 dB/m using a pump beam with NA=0.0377 to prevent losses due to vignetting.

The output characteristics of the laser are shown in Fig. 7 for two values of pump beam aperture adjusted using the diaphragm in the optical beam shaping unit. Though a decrease of the diaphragm diameter reduces the available pump, as expected, the output power at a specific pumping rate increases, demonstrating improvement in pumping efficiency due to reduced vignetting and increased pump absorption in the active core.

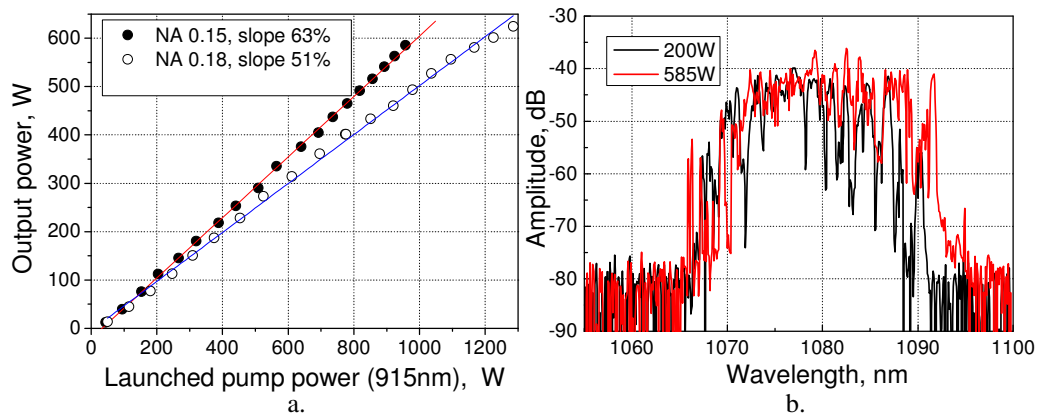


Fig. 7. Output characteristics of laser: (a) Output power versus launched pump power. The solid circles correspond to a pump beam with NA=0.15 and the open circles to pump with NA=0.18. (b) Spectrum of output radiation, pump beam with NA=0.15.

Consequently, the slope efficiency is 63% for a pump beam of NA=0.15, and reduces down to 51% for NA=0.18 (Fig. 7 (a)). The maximum achieved power was 624 W. The laser emits a broad spectrum with a FWHM bandwidth of 20 nm, as shown in Fig. 7 (b).

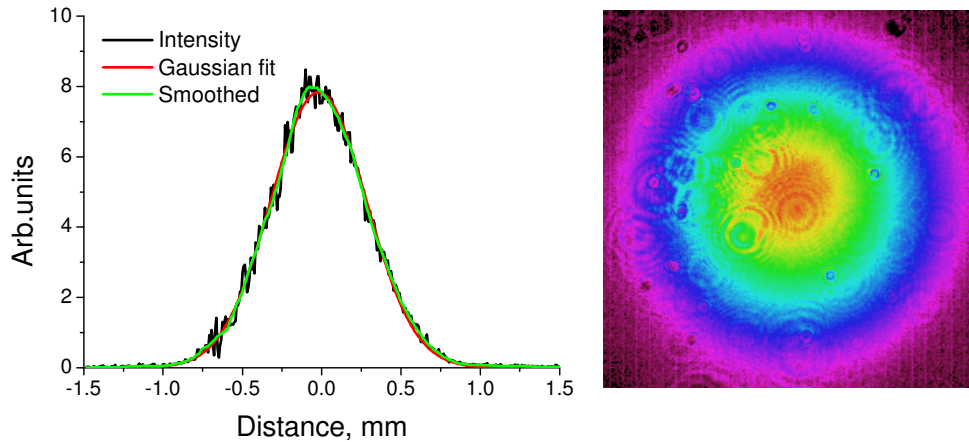


Fig. 8. Output beam profile with $M^2=1.08$.

Beam profile and two-dimensional intensity distribution of output beam are shown in Fig. 8. The laser operates on the fundamental mode with $M^2=1.08$.

4. Discussion

The important experimental observation, supported by the analysis, is that efficient optical pumping can be achieved even with pump beam apertures significantly exceeding the critical value needed for vignetting-free propagation. The significant practical result of this conclusion is the possibility for optical pumping with low-brightness sources, e.g. diode bars. The experimental dependence of slope efficiency on the numerical aperture of the launched pump beam (Fig. 7 (a)) is in good agreement with results of modeling presented in Fig. 5. The modeling of the tapered double clad amplifier presented here identifies the features and optimal design of the fiber for efficient operation. The fraction of pump power which leaks from the T-DCF due to vignetting increases with pump beam NA, resulting in slope efficiency deterioration. Therefore, to prevent the degradation of pumping efficiency with high-NA pump sources, a substantial fraction of the pump power should be absorbed in the active core well before vignetting sets in.

It is demonstrated that absorption for a Lorentzian pump beam with $NA=0.15$ reaches 15 dB and is sufficient for practical laser operation. However, a further increase in the beam NA up to 0.18 causes an increase in launched pump power (up to 1.3 kW, Fig. 7 (a)), is accompanied by a reduction in pump absorption (from 15 to 13.37 dB) and leads to slope efficiency reduction (Fig. 7). However, a practically acceptable value of absorption could be achieved even with higher NA pump sources, for highly-doped core fiber with a large value of paraxial absorption. Fig. 5 demonstrates 17.2 dB absorption for a beam with $NA=0.22$). This observation demonstrates the potential of high-NA pump sources for highly-doped T-DCF.

The analysis identifies key parameters responsible for pump absorption in tapered fiber, namely in-core absorption, cross-sectional geometry and longitudinal shape of the taper. The influence of paraxial ray absorption presented in Fig. 5 shows that the effect of vignetting becomes more significant for low paraxial ray absorption. Thus, the T-DCF absorption increases from 8 dB to 22.3 dB when the axial ray absorption increases from 0.5 dB/m to 2 dB/m, as shown in Fig. 5 for pumping with the beam having NA of 0.15. Another major parameter is the axial shape of the T-DCF, which affects its pump absorption dramatically since it determines the normalized vignetting length (Eqs.(11)). The profile of the T-DCF used in experiments, and the corresponding axial dependence of local taper angle proportional to the first derivative of diameter, are shown in Fig. 9 (red curves). It can be seen that the local cone angle is small at the large-core end of the taper and experiences a strong increase over the first 4 m, up to 200 μ rad, followed by near exponential reduction. This rapid increase of

the local taper angle may be accompanied by significant losses due to vignetting, because this feature occurs at the very outset of the taper, where the unabsorbed pump power is high. The shape of T-DCF used in this study could, therefore, be improved, e.g. by using a design in which local taper angle gradually increases with length, achieving the maximum when a substantial part of the pump power is absorbed, i.e. a parabolic taper or a linear taper with constant cone angle.

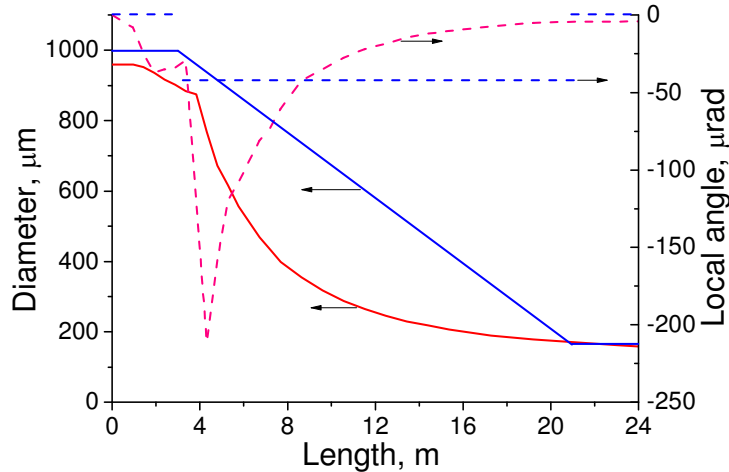


Fig. 9. Shape of the taper: diameter (solid line) and local angle (dashed line) as function of the length; red color – actual T-DCF used in the experiment, blue color – a hypothetical linear T-DCF.

An example of a linear taper with a constant cone angle of $46 \mu\text{rad}$ is shown in Fig. 9 (blue curves). The pump absorption as a function of numerical aperture of launched pump beam for these T-DCFs, calculated using Eq. (12a), is presented in Fig. 10. The results plotted in Fig. 10 demonstrate the crucial role of taper shape in pump absorption. Thus, the T-DCF with linear fiber diameter length dependence exhibits an absorption increase of $\sim 6 \text{ dB}$ compared with the taper of the same length used in this study, with the same pump beam aperture of 0.22.

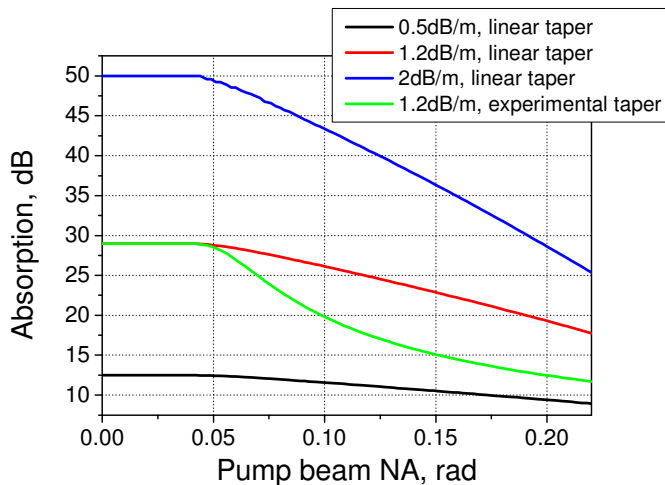


Fig. 10. Pump absorption versus numerical aperture of launched pump beam for linear T-DCF (corresponding to Fig. 9, blue curves) for different paraxial ray absorption, 0.2 dB/m (black curve), 1.2 dB/m (red) and 2 dB/m (blue). The green curve corresponds to the experimental T-DCF.

This result allows us to conclude that T-DCF with sufficient paraxial ray absorption and optimized longitudinal shape can operate efficiently under overfill launch conditions using low-brightness, high-NA, pump sources. It is expected that power scaling using tapered double-clad fiber technology can be achieved in the future, by implementation of the following:

- Enlargement of the T-DCF diameter. Current fiber technology is capable of producing T-DCF with a 2 mm large-end diameter, which would allow the launch of a few kilowatts of pump power [10];
- Increase of the mode field diameter would improve the energy storage capability of the fiber. Tapered active large-core microstructured fiber [11] or multicore fiber [12] hold significant potential for power scaling.

5. Conclusion

We have investigated the performance and major parameters governing the operation of tapered double-clad fiber amplifiers both theoretically and experimentally. A ray optics analysis applied to this fiber reveals good agreement with experimental observations. Paraxial ray absorption in the fiber core and the longitudinal shape of the tapered fiber have been found to be the major factors affecting the amplifier characteristics. The analysis and measurements show that low brightness sources with high numerical apertures can be used for efficient pumping of the tapered fiber, offering both high launching efficiency and low pump power losses. This is an important practical conclusion which opens up the opportunity of using high-power, cost-effective diode bars. Using this innovative design concept, we developed a single mode ($M^2=1.08$) ytterbium fiber laser with power exceeding 600 W. The potential of this approach for scaling to higher powers has been discussed.